RSC Advances

PAPER

View Article Online
View Journal | View Issue

Cite this: *RSC Adv.*, 2025, **15**, 40093

Repurposing disposable medical syringes into valuable fluorescent carbon dots: application to the fluorometric determination of nintedanib

Mohamed N. Goda,[a] Laila S. Alqarni,[a] K. S. Al-Namshah,[a] Hossieny Ibrahim,[b] Al-Montaser Bellah H. Ali[c] and Mohamed M. El-Wekil *[c]

Monitoring nintedanib (NTB) using reliable analytical methods is essential for ensuring safe dosing, minimizing toxicity, assessing drug–drug interactions, and supporting quality control in personalized cancer therapy. In this work, we present a cost-effective and energy-efficient hydrothermal strategy for synthesizing nitrogen-doped carbon dots (CDs) from disposable plastic syringes. The process, carried out at 200 °C following a calcination pretreatment, not only provides a sustainable route for valorizing biomedical waste but also addresses pressing environmental challenges. The as-prepared CDs exhibited intense green fluorescence, outstanding photostability, and a high quantum yield of 46.42%, reflecting their superior optical performance. Upon exposure to NTB, a concentration-dependent quenching response at 470 nm was observed, primarily mediated by the inner filter effect (IFE). This mechanism enabled highly sensitive NTB detection, with an ultralow detection limit of 2.5 nM (S/N = 3). The probe demonstrated remarkable selectivity, showing negligible interference from common coexisting ions, biomolecules, and anticancer drugs. Analytical accuracy was validated by recovery studies in spiked serum and urine samples, which ranged from 97.6% to 103.2%, while RSD values below 3.48% confirmed excellent precision and reproducibility. These findings establish the proposed CD-based probe as a robust, reproducible, and clinically relevant tool for NTB quantification. By demonstrating the conversion of discarded medical plastics into high-value nanomaterials, this work presents a strategy that aligns with the goals of green nanotechnology and delivers a practical platform for bioanalytical sensing, therapeutic drug monitoring, and pharmacokinetic studies. The dual focus on waste repurposing and clinical utility underscores the potential the potential of syringe plastic-derived CDs for translation into next-generation biomedical diagnostics.

Received 22nd September 2025
Accepted 16th October 2025

DOI: 10.1039/d5ra07196h

rsc.li/rsc-advances

1 Introduction

Nintedanib (NTB), a multi-target tyrosine kinase inhibitor, was initially approved for idiopathic pulmonary fibrosis and later for systemic sclerosis-associated and other progressive fibrosing interstitial lung diseases. Beyond its capacity to attenuate lung function decline, NTB represents a paradigm shift in antifibrotic therapy by simultaneously targeting multiple signaling cascades implicated in aberrant fibroblast activation, tissue remodeling, and angiogenesis.[1,2] Mechanistically, NTB inhibits multiple receptor tyrosine kinases. This broad inhibition translates into suppression of fibroblast proliferation, reduced extracellular matrix deposition, and modulation of pro-inflammatory pathways. Emerging evidence also suggests potential roles of NIN in oncology and other fibrotic disorders, highlighting its therapeutic versatility and prompting ongoing investigations into biomarker-guided patient stratification and combination regimens with immunomodulatory or anti-inflammatory agents.[3,4] Most analytical approaches reported for the quantification of NTB rely on chromatographic techniques.[5–8] While these methods offer high specificity, they are often associated with considerable drawbacks such as high operational costs, labor-intensive sample preparation, and the use of toxic organic solvents that pose environmental concerns. These limitations restrict their practicality for routine quality control, particularly in resource-limited settings. Consequently, there is a pressing need for the development of alternative analytical platforms that are not only rapid, sensitive, and cost-effective but also sustainable and compatible with green chemistry principles.

Discovered in 2004, CDs emerged during single-walled carbon nanotube purification,[9] have since emerged as a versatile class of fluorescent nanomaterials. Their unique

[a]*Department of Chemistry, College of Science, Imam Mohammad Ibn Saud Islamic University (IMSIU), Riyadh 11623, Saudi Arabia*
[b]*School of Biotechnology, Badr University in Assiut, Assiut 2014101, Egypt*
[c]*Department of Pharmaceutical Analytical Chemistry, Faculty of Pharmacy, Assiut University, Assiut, Egypt. E-mail: mohamed.elwakeel@pharm.aun.edu.eg; mohamed.mohamoud@ymail.com*

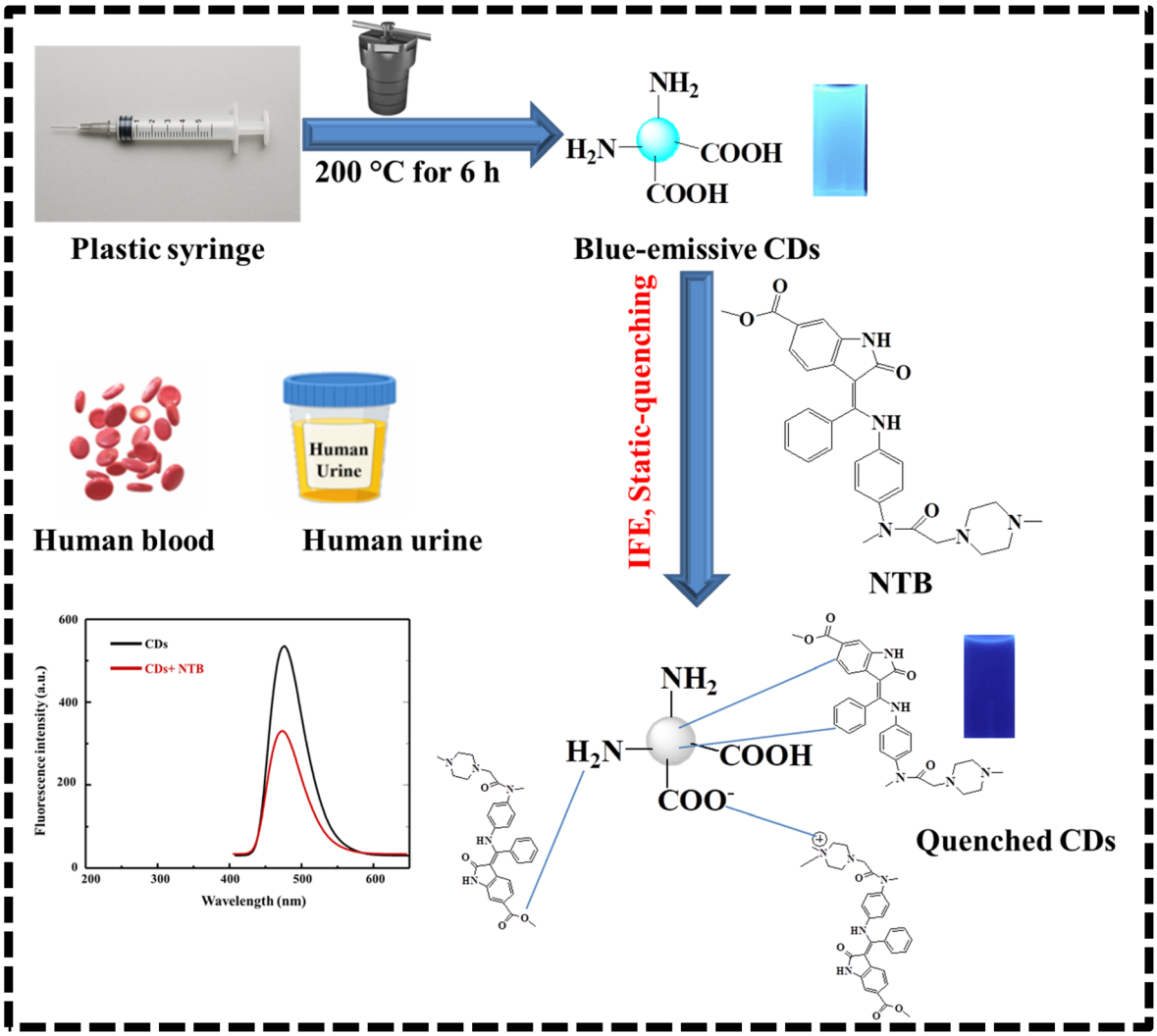

Scheme 1 Preparation of plastic syringe -derived CDs for detection of NTB.

photoluminescent properties enable applications across a wide spectrum, including the detection of metal ions, biomolecules, and pharmaceuticals, as well as monitoring of environmental pollutants, temperature fluctuations, and pH variations.[10,11] The widespread utility of CDs is attributed to their favorable physicochemical characteristics, such as strong and tunable luminescence, excellent aqueous solubility, chemical stability, biocompatibility, high quantum yield, and inherently low toxicity.[12,13] Synthesis of CDs can be achieved through both top-down strategies (*e.g.*, arc discharge, laser ablation, electrochemical oxidation) that cleave bulk carbon structures, and bottom-up routes (*e.g.*, hydrothermal treatment, microwave-assisted synthesis, pyrolysis, solvothermal carbonization) that assemble nanodots from molecular precursors.[14] Ongoing research increasingly emphasizes green and waste-derived synthesis, integrating sustainability into CD fabrication while broadening their scope in bioimaging, optoelectronics, photocatalysis, and environmental remediation.

The COVID-19 pandemic triggered an unprecedented rise in the consumption of single-use medical plastics, including masks, gloves, gowns, and diagnostic kits, resulting in a dramatic escalation of biohazardous waste generation.[15,16] Inadequate segregation, collection, and disposal practices not only strain existing waste management infrastructure but also heighten the risk of secondary pathogen transmission and environmental contamination. This situation underscores the urgent need for robust, sustainable biomedical waste management systems that integrate safe handling, advanced treatment technologies, and circular economy principles.[17,18] Hospital-derived single-use plastics, which are predominantly carbon-rich polymers, have recently been recognized as promising feedstocks for the synthesis of fluorescent carbon dots (CDs).[19,20] Converting biomedical plastic wastes into value-added nanomaterials provides a dual benefit: it alleviates the environmental burden of plastic pollution and generates functional nanostructures with broad utility. The resulting CDs possess distinctive optical, chemical, and biocompatible properties, making them promising candidates for applications in bioimaging, photocatalysis, pollutant degradation, and sensing. For instance, Li *et al.* converted discarded medical masks into blue-emitting CDs, which were successfully applied for the detection

of Fe^{3+} ions and sodium hydrosulfite.[19] Similarly, Kumari *et al.* reported the recycling of medical wastes such as gloves, masks, and syringes into fluorescent markers.[20] The concept of waste valorization—transforming hazardous or low-value waste materials into high-value functional products—offers a compelling strategy to address both environmental and technological challenges. In this context, converting medical plastic waste into fluorescent carbon dots enables a dual-purpose solution: mitigating plastic pollution while producing functional nanomaterials for biomedical applications. This approach is aligned with the principles of green chemistry, reducing reliance on toxic reagents and enhancing the sustainability of nanomaterial synthesis. Although CDs have been previously synthesized from materials such as masks and gloves,[19,20] limited research has focused on repurposing syringe plastics, and none has targeted the selective detection of NTB using such waste-derived CDs.

In this study, we introduce a sustainable and facile strategy to upcycle discarded medical syringes into highly fluorescent carbon dots (CDs) with finely tuned optical properties. Processing at temperatures exceeding 100 °C not only promotes efficient carbonization but also ensures complete inactivation of potential pathogens, thereby enabling the safe reuse of biohazardous plastic waste. The as-synthesized CDs display strong and stable fluorescence without the need for additional surface passivation, alongside excellent photostability and inherent biocompatibility. Their analytical potential was validated through the selective and sensitive detection of NTB, with reliable performance in biological matrices and a markedly shortened response time (Scheme 1). Beyond analytical sensing, this waste-to-nanomaterial approach presents a cost-effective and environmentally responsible pathway to transform hospital plastics into multifunctional nanostructures, reinforcing both ecological sustainability and biomedical innovation.

2 Experimental

2.1 Materials and reagents

NTB (99.9%) was kindly provided by Boehringer Ingelheim (Cairo, Egypt). Reference compounds including ascorbic acid (98.7%), dopamine (97.7%), histidine (97.8%), arginine (98.8%), glucose (97.6%), glutathione (98.7%), cysteine (97.8%), lysine (97.3%), alanine (97.9%), pirfenidone (98.4%), methotrexate (97.8%), oxaliplatin (99.7%), carboplatin (98.9%), cisplatin (97.9%), and capmatinib (98.9%) were purchased from Sigma-Aldrich (Germany). Analytical-grade reagents such as monobasic sodium phosphate, dibasic sodium phosphate, hydrochloric acid, sodium hydroxide, and various metal salts were supplied by Merck (Germany). Single-use syringe waste was collected under approved protocols from Assiut University Hospital (Assiut, Egypt) and thoroughly pre-treated prior to use. Throughout the study, deionized water of high purity was employed for all preparations and experimental procedures.

2.2 Instrumentation

Details of instruments and samples preparation are included in the SI.

2.3 Preparation of CDs

Disposable syringe waste was systematically collected, sanitized, and converted into CDs through a two-step carbonization process involving thermal calcination followed by hydrothermal treatment. Initially, syringe fragments were placed in silica crucibles and subjected to calcination in a muffle furnace at 280 °C for 3 h to promote primary carbonization and pathogen inactivation. The obtained carbonaceous residues were dispersed in 15 mL of deionized water and subsequently transferred into a Teflon-lined stainless-steel autoclave for hydrothermal processing at 200 °C for 6 h. Post-treatment, the suspensions were centrifuged at 6000 rpm for 20 min to eliminate residual particulates. The clear supernatants were dialyzed (MWCO 2000 Da, 24 h) against deionized water to remove low-molecular-weight impurities and further purified by ultracentrifugation. The resulting highly fluorescent CDs were collected as solid extracts, dried, and stored at room temperature until characterization and application.

2.4 Detection steps

For fluorescence measurements, varying concentrations of NTB (300 μL) were combined with 400 μL of CDs (100 μg mL^{-1}) and 300 μL of phosphate buffer solution (0.1 M, pH 7.4). The mixtures were gently mixed and incubated at 25 °C for 1 min to allow interaction between NTB and the CDs. Fluorescence emission spectra were then recorded at 470 nm following excitation at 370 nm, with both excitation and emission slit widths set to 3 nm.

2.5 Selectivity studies

To evaluate the selectivity of the proposed sensing system, 300 μL of ten-fold higher concentrations of potential interfering species (including common ions, biomolecules, and anticancer drugs) were mixed with 400 μL of CDs (100 μg mL^{-1}) and 300 μL of phosphate buffer (0.1 M, pH 7.4). The mixtures were gently vortexed and incubated at 25 °C for 1 min to facilitate possible interactions. Fluorescence emission spectra were subsequently recorded at 470 nm upon excitation at 370 nm, with both excitation and emission slit widths maintained at 3 nm.

3 Results and discussions

3.1 Characterization

The structural characteristics of the as-prepared CDs were systematically validated using XRD, FTIR, and TEM analyses. TEM micrographs (Fig. 1A) demonstrated uniformly dispersed, quasi-spherical nanoparticles with diameters ranging from 2.2 to 6.1 nm, yielding an average size of 3.8 ± 0.17 nm (Fig. 1B). High-resolution TEM further revealed distinct lattice fringes with an interplanar spacing of 0.23 nm, which can be attributed to the (002) crystallographic plane of graphitic carbon.[21] This observation corroborates the partially ordered sp^2-hybridized domains within the CDs, a structural feature frequently associated with their enhanced photoluminescence and electronic conductivity. Notably, such graphitic domains are critical for facilitating π–π interactions, surface passivation, and charge

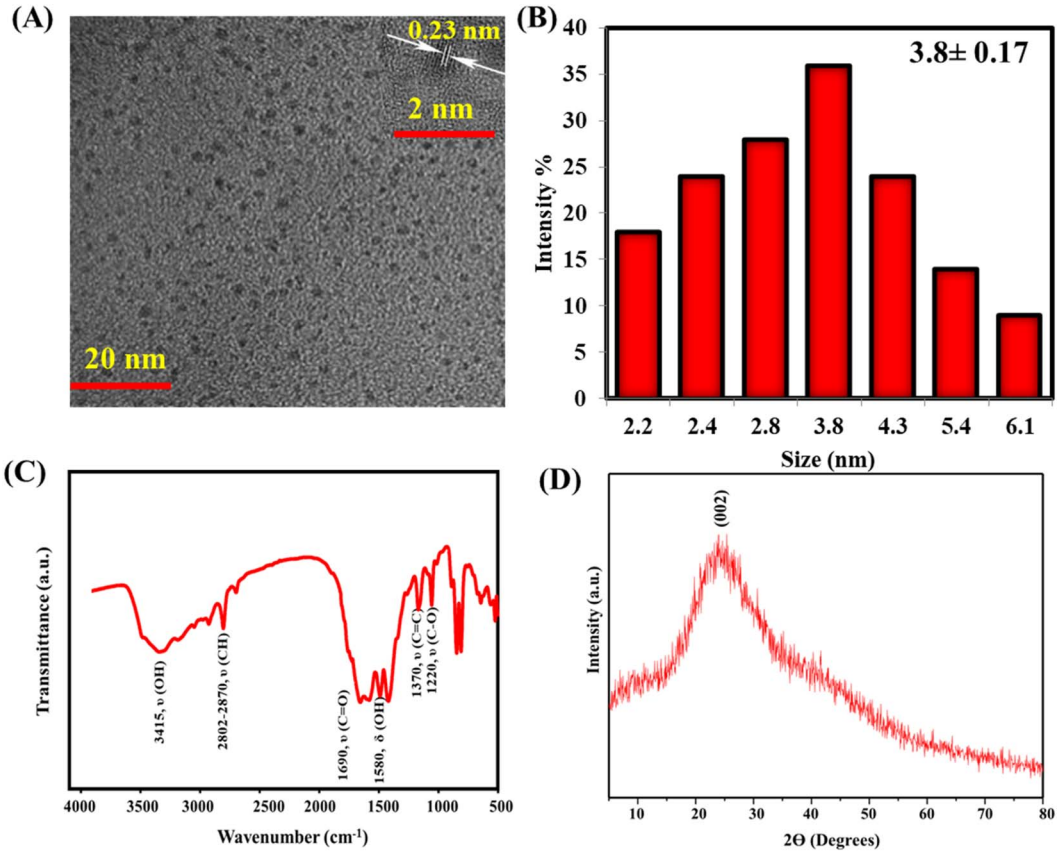

Fig. 1 SEM (A), size distribution (B), FTIR (C), and XRD pattern of plastic syringe -derived CDs.

transfer processes, which collectively underpin the superior optical performance and potential catalytic applications of CDs.[22]

The FTIR spectrum of the synthesized CDs confirmed the presence of diverse surface functional groups, indicative of successful surface passivation and heteroatom incorporation (Fig. 1C). A broad absorption band centered at 3415 cm^{-1} was assigned to O–H/NH stretching vibrations, reflecting hydroxyl groups and adsorbed water molecules, which enhance aqueous dispersibility and hydrogen-bonding interactions. The absorptions at 2802 and 2870 cm^{-1} corresponded to aliphatic C–H stretching, suggesting the presence of alkyl moieties on the CD surface. A sharp, intense band observed at 1690 cm^{-1} was attributed to C=O stretching of carbonyl or carboxyl groups, while additional peaks at 1580, 1370, and 1220 cm^{-1} were associated with C=C, OH/NH, and C–O stretching vibrations, respectively.[23,24] Collectively, these findings confirm that the CDs are decorated with oxygenated and partially conjugated surface functionalities, which not only improve colloidal stability but also provide abundant reactive sites for further chemical modification, metal ion coordination, or biomolecular interactions—key attributes for their prospective applications in sensing, catalysis, and bioimaging.

The XRD pattern of the synthesized CDs revealed a broad diffraction peak centered at ~23.1°, corresponding to the (002) plane of graphitic carbon (Fig. 1D). The broad nature of this peak reflects the low crystallinity and limited long-range order of the sp^2 domains. These findings are consistent with the structural features observed in the HRTEM analysis.

XPS analysis confirmed the elemental composition and chemical states of the synthesized CDs. The survey spectrum (Fig. 2A) showed prominent C, N, and O signals. In the high-resolution C 1s spectrum (Fig. 2B), peaks at 283.5 eV and 286.1 eV were attributed to C=C/C–C and C=O groups, respectively. The N 1s spectrum (Fig. 2C) revealed peaks at 395.3, 396.8, and 399.4 eV, corresponding to C–N, CH–N, and C=N. The O 1s spectrum (Fig. 2D) showed peaks at 534.3, 534.6, and 536.4 eV, assigned to C–O, C–OH, and C=O functionalities. These oxygen and nitrogen-rich surface functionalities are known to improve the hydrophilicity and colloidal stability of CDs, thereby facilitating their potential use in aqueous environments and biological systems.

Fig. S1A presents the EDX spectrum of the as-synthesized CDs, confirming carbon, nitrogen, and oxygen as the principal constituents. The relatively high oxygen content suggests the presence of abundant surface functional groups, which are expected to improve solubility and chemical reactivity in aqueous environments. Complementary structural insights were obtained from Raman spectroscopy (Fig. S1B). The spectrum displayed two well-defined features: a D band at ~1352 cm^{-1}, corresponding to disordered sp^3-hybridized carbon, and a G band at ~1578 cm^{-1}, attributed to graphitic sp^2 domains. The

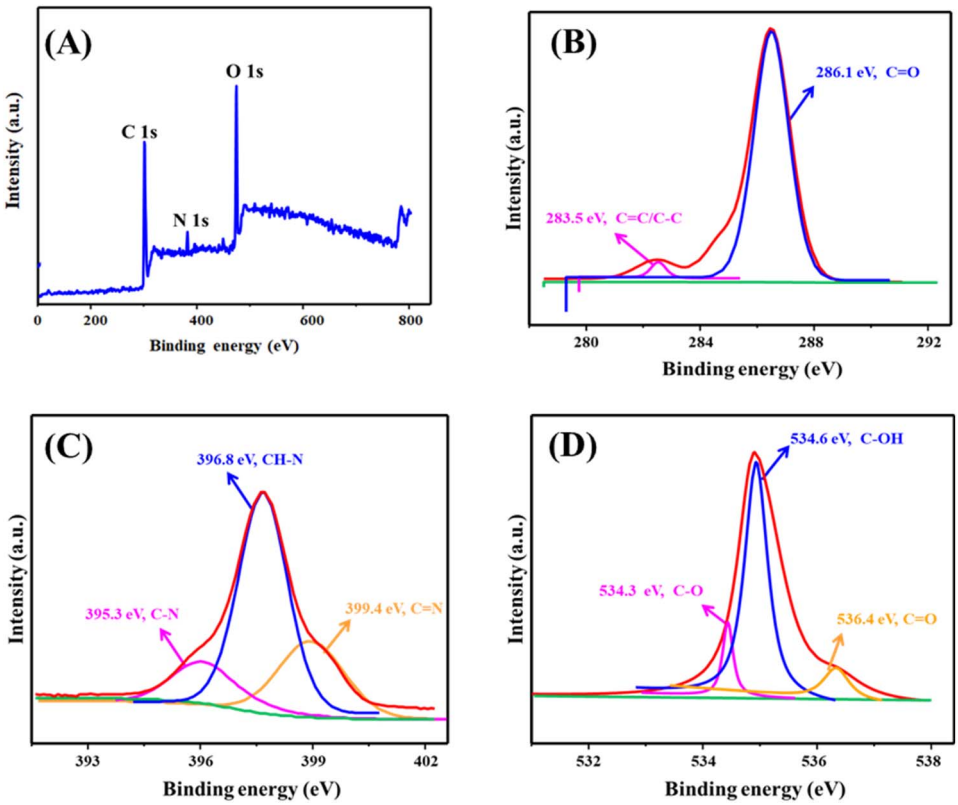

Fig. 2 (A) Full XPS survey of plastic syringe -derived CDs; (B–D) deconvoluted spectra of C 1s, N 1s, and O 1s, respectively.

calculated intensity ratio (I_D/I_G) of 1.26 reflects a defect-rich and largely amorphous carbon framework composed of both sp^2 and sp^3 domains. Such structural heterogeneity is known to introduce emissive defect states that enhance the photoluminescence of CDs, while the remaining graphitic regions preserve favorable electronic and optical characteristics. This synergistic interplay between disorder-induced states and sp^2 conjugation underpins the suitability of CDs for high-performance fluorescence sensing and bioimaging applications.[25]

Zeta potential measurements were conducted to evaluate the surface charge and colloidal stability of the synthesized CDs. As shown in Fig. S1C, the zeta potential was determined to be −22.18 mV. The negative surface charge is primarily attributed to the abundance of oxygen-containing functional groups, such as –COOH and –OH moieties.[26,27] The moderately high negative value indicates strong electrostatic repulsion between particles, thereby preventing aggregation and ensuring good colloidal stability in aqueous dispersions. Such stability is particularly advantageous for applications in biological and environmental systems, where long-term dispersion and surface reactivity are critical.

The specific surface area and porosity of the synthesized CDs were investigated by N_2 physisorption at 77 K under a saturated vapor pressure of 100.95 kPa. The adsorption–desorption isotherms exhibited a characteristic type IV profile with pronounced hysteresis loops (Fig. S1D), confirming the presence of mesoporous structures. The Brunauer–Emmett–Teller (BET) surface area was calculated to be 7.98 $m^2\ g^{-1}$, with pore diameters distributed between 4–11 nm and an average pore size of 5.74 nm. The total pore volume was determined to be 0.00153 $cm^3\ g^{-1}$. Although the BET surface area of the CDs was measured to be 7.98 $m^2\ g^{-1}$—relatively low compared to activated carbons—the adsorption–desorption isotherms revealed a type IV profile with hysteresis, characteristic of mesoporous materials. The pore size distribution (4–11 nm) suggests the presence of mesopores that, while limited in number, can facilitate diffusion of NTB molecules and promote accessibility to surface active sites. Such mesoporosity may contribute to the rapid and efficient quenching behavior observed, despite the low overall surface area. These structural features thus support the CDs' suitability for bioanalytical applications, particularly in aqueous sensing environments.

The UV-vis absorption spectrum of the synthesized CDs displays two prominent bands centered around 232 nm and 346 nm (Fig. S2A). These features are commonly observed in carbonaceous nanomaterials and are often associated with π–π transitions of C=C bonds* and *n–π transitions involving lone pairs on heteroatoms (*e.g.*, C=O, C=N), respectively. However, it is important to note that CDs lack well-defined conjugated systems found in conventional molecular fluorophores, and their absorption profile likely arises from a mixture of sp^2 clusters, surface defects, and heteroatom dopants. Additionally, a shoulder in the UV region may be attributed to localized surface plasmon resonance (SPR)-like effects, particularly in the presence of extended aromatic domains or dopant clusters.

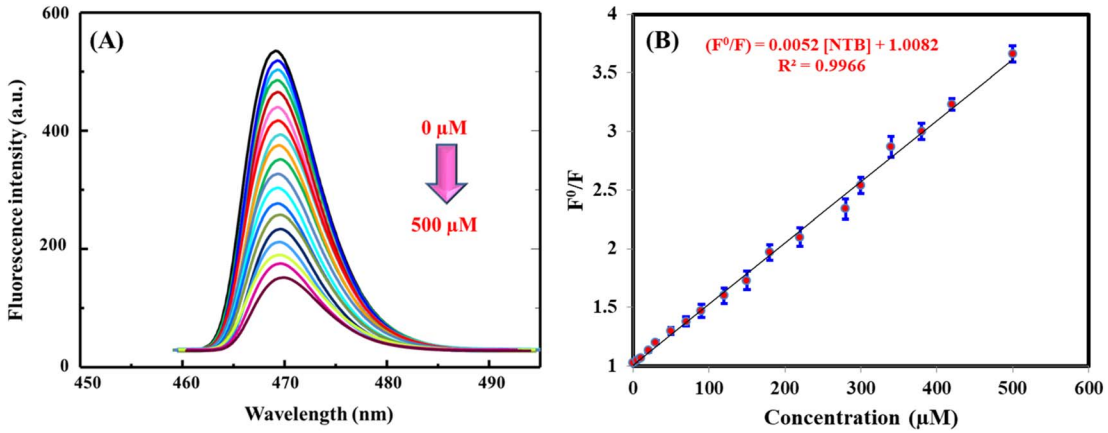

Fig. 3 (A) Fluorescence responses of CDs upon addition NTB (0–500 μM) and (B) corresponding calibration plot. Conditions are CDs' concentration is 100 μg mL^{-1}, pH 7.4, and incubation time is 1 min.

These combined effects reflect the complex and heterogeneous electronic structure of the CDs. Upon excitation at 370 nm, the CDs exhibited a strong emission peak at 470 nm, with excitation-independent fluorescence observed in the range of 340–390 nm (Fig. S2B). This stable blue emission was further confirmed by chromaticity diagram (Fig. S2C). The absolute photoluminescence quantum yield, measured using quinine sulfate as a reference, was calculated to be 46.42%. Such a relatively high quantum yield, combined with excitation-independent behavior and stable blue fluorescence, underscores the suitability of CDs for applications in bioimaging, light-emitting devices, and fluorescence-based sensing.

The synthesized CDs exhibited remarkable environmental stability under diverse external conditions. As shown in Fig. S3A, fluorescence intensity remained unaffected even at NaCl concentrations up to 2.5 M, demonstrating strong ionic resistance. High photostability was further confirmed under continuous UV irradiation for 180 minutes, with negligible loss of emission intensity (Fig. S3B). The CDs also retained stable fluorescence across a broad pH range of 4–10, with only minor quenching under strongly acidic or alkaline environments due to protonation or deprotonation of surface groups (Fig. S3C). Temperature-dependent studies revealed consistent emission from 25–90 °C (Fig. S3D), highlighting robust thermal tolerance. In addition, no evidence of photobleaching or aggregation was observed after 50 days of storage under ambient conditions (Fig. S3E). Collectively, these results confirm the excellent chemical, thermal, and photophysical stability of CDs, which is essential for their integration into real-world applications such as long-term sensing, bioimaging, and optoelectronic devices.

3.2 Quenching mechanism

The fluorescence quenching mechanism of plastic syringe-derived CDs by NTB was systematically examined using spectroscopic and physicochemical analyses. It is worth noting that NTB does not exhibit intrinsic fluorescence under the chosen excitation wavelength (λ_{ex} = 370 nm). Therefore, no significant spectral interference or emission overlap is expected from NTB itself. However, its strong absorbance in the 320–390 nm range overlaps with the excitation band of the CDs, strongly suggesting that the observed quenching arises primarily from the inner filter effect (IFE), rather than energy transfer or fluorescence competition (Fig. S4A). Time-resolved fluorescence measurements further support this conclusion, as the average lifetime of CDs exhibited only a marginal decrease from 7.76 ns to 7.65 ns upon NTB addition (Fig. S4B), effectively ruling out dynamic quenching processes.[28] Complementary zeta potential measurements revealed substantial differences in surface charge (−22.18 mV for CDs and +4.19 mV for NTB; Fig. S4C), indicative of electrostatic repulsion that prevents stable ground-state complexation, thereby strengthening the IFE hypothesis.[29] Moreover, Stern–Volmer analysis (Fig. S46D) demonstrated a temperature-dependent decline in the quenching constant (K_{sv}), consistent with static-type interactions.[30] To unequivocally decouple the IFE from static quenching, we have now performed the recommended control experiment. We selected an excitation wavelength of 480 nm, where the absorption of NTB is negligible, while the CDs exhibit emission. A significant fluorescence quenching was still observed, confirming that a static quenching mechanism *via* ground–state complex formation is the primary contributor. The residual IFE observed at 370 nm excitation likely provides an additional, secondary quenching effect.

3.3 Optimization of conditions

The synthesis of CDs derived from syringe plastic was systematically optimized by evaluating the influence of key parameters, namely reaction temperature and duration (Fig. S5). The fluorescence response served as the primary criterion for optimization. Among the tested conditions, a reaction temperature of 200 °C combined with synthesis duration of 6 h yielded CDs with the highest emission intensity, highlighting the critical role of both thermal energy and reaction time in dictating the formation of emissive surface states. These optimized conditions likely promote efficient carbonization and surface

passivation, which are essential for generating stable luminescent centers.

Detection parameters were further optimized to maximize the analytical performance of syringe-derived CDs toward NTB (Fig. S6). Three factors were systematically evaluated: CD concentration (20–200 μg mL^{-1}), solution pH (5–9), and incubation time (0.5–5 min). As shown in Fig. S6A, fluorescence intensity increased with CD concentration up to 100 μg mL^{-1}, beyond which the signal plateaued, suggesting saturation of binding sites without notable aggregation or self-quenching effects. The strongest response was observed at physiological pH (7.4; Fig. S6B), where the partial protonation of NTB amine groups (p*K*a ≈ 7.9) and deprotonation of CD surface carboxyl groups (p*K*a ≈ 4.3) favor electrostatic attraction. These interactions are further stabilized by hydrogen bonding and π–π stacking between NTB's aromatic moieties and the sp^2 domains of CDs. Shifts away from pH 7.4 altered protonation equilibria, thereby weakening these supramolecular interactions. Kinetic studies (Fig. S6C) revealed that maximum fluorescence quenching was achieved within 1 min, with no additional gain upon prolonged incubation, confirming fast association and strong affinity between CDs and NTB. On this basis, a concentration of 100 μg mL^{-1} CDs, physiological pH, and 1 min incubation were selected as the optimal conditions for subsequent sensing assays.

3.4 Quantitative data

The fluorescence response of CDs toward nintedanib (NTB) was systematically investigated under optimized assay conditions over a concentration range of 0–500 μM. As depicted in Fig. 3A, progressive quenching of CD fluorescence was observed with increasing NTB concentration, reaching 33.7% reduction at 500 μM. The Stern–Volmer analysis yielded a robust linear relationship, expressed as: $F^0\ F^{-1} = 1.0082 \pm 0.17 \times 10^{-7} + 0.0052\ C_{NTB}$, where F^0 and F represent the fluorescence intensities in the absence and presence of NTB, respectively. The regression exhibited excellent linearity ($R^2 = 0.9966$) with minimal residual deviation and no significant lack-of-fit ($p > 0.05$), confirming the model's reliability. The high correlation coefficient underscores the precision of the CD–NTB interaction, suggesting a predictable quenching mechanism that may involve static complex formation. The analytical sensitivity of the proposed method was assessed by calculating the detection limit (LOD) and quantitation limit (LOQ) using the conventional signal-to-noise criteria of 3 : 1 and 10 : 1, respectively. The LOD was determined to be 0.0025 μM, while the LOQ was 0.01 μM (Fig. 3B). These values demonstrate that the system is capable of detecting NTB at trace concentrations with high reliability (Table 1). Such sensitivity highlights the potential of CDs as fluorescence probes for therapeutic monitoring of NTB (C_{max} = 0.042 μM after 100 mg oral administration),[36] especially considering the drug's narrow therapeutic index in clinical oncology. Importantly, the absence of systematic bias in the regression analysis indicates that the quenching effect is reproducible and not influenced by experimental artifacts.

Table 1 Comparative analysis of key analytical parameters for NTB detection using the proposed method *versus* existing reported techniques

Technique	Linear range (μM)	LOD (μM)	Reference
HPLC/UV	3.7–277.8	—	5
	18.5–92.5	—	6
UPLC-MS/MS	0.0018–37.04	—	31
	0.00018–92.5	0.00018	32
Electrochemical	0.01 to 0.40	0.0037	33
	0.05–6.2	0.002	34
Fluorometry			
N-CQDs	1.85–37.03	0.81	35
Syringe plastic-derived CDs	0.01–500	0.0025	This work

3.5 Precision

Method precision was comprehensively evaluated at three representative NTB concentrations (2.0, 10.0, and 50.0 μM). Both within-day and between-day experiments demonstrated relative standard deviation (RSD) values consistently below 3.46% (Table 2). These low deviations confirm excellent reproducibility of the assay across different concentration levels and measurement intervals. The results are well within the acceptance limits outlined in the ICH M10 bioanalytical method validation guidelines, which permit RSD values up to 15% across the calibration range. The high reproducibility not only validates the robustness of the proposed method but also ensures its reliability for long-term application in routine analysis.

3.6 Reproducibility and selectivity/anti-interference studies of the probe

The reproducibility of the proposed sensing platform was evaluated by analyzing the fluorescence responses of seven independently fabricated probes, all synthesized under identical experimental conditions. As shown in Fig. S7, the relative standard deviation (RSD) values across these parallel preparations did not exceed 3.09%, demonstrating excellent batch-to-batch consistency. Such a low variation underscores the reliability of the as-prepared CDs and the robustness of the fabrication procedure. The results further indicate that the synthetic route is well controlled, minimizing structural or surface heterogeneity among different batches. This level of reproducibility is crucial for ensuring consistent performance in practical applications, particularly when scaling up for bioanalytical assays, clinical diagnostics, or point-of-care testing.

The selectivity of the sensing system was systematically investigated using 50 μM NTB in the presence of a 10-fold molar excess of potential interferents, including inorganic ions, biomolecules, and structurally related anticancer drugs. As shown in Fig. 4, only NTB produced a pronounced quenching response, whereas the other tested species caused negligible changes in fluorescence. Minor quenching was observed for certain basic amino acids (lysine, arginine, and histidine), which can be attributed to transient electrostatic interactions with the negatively charged surface groups of the CDs. However, this effect was readily mitigated by simple dilution, and co-

Table 2 Precision of the CDs-based fluorometric method for detecting NTB ($n = 6$)

	Within day precision			Between days precision		
Concentration (μM)	Found (μM)	Recovery %	RSD %	Found (μM)	Recovery %	RSD %
2.0	2.05	102.5	1.87	1.94	97.0	3.46
10.0	9.97	99.7	3.00	10.27	102.7	2.98
50.0	48.97	97.9	2.64	52.61	105.2	3.09

incubation experiments confirmed that the presence of these interferents did not alter the NTB-induced quenching response. Specifically, the fluorescence intensity in mixtures of NTB with excess interferents was indistinguishable from that observed with NTB alone, demonstrating that the probe's signal is highly specific to NTB. The probe exhibited notable selectivity, even though many interfering species exhibit absorbance in the 340–380 nm range. This observation suggests that additional supramolecular interactions—including electrostatic attraction, π–π stacking, and hydrogen bonding—may promote NTB-CDs affinity, thereby enhancing quenching selectively. While these interactions may not induce strong static complex formation, they can modulate the effective proximity and interaction duration, indirectly contributing to preferential IFE-based quenching. Thus, we propose a hybrid model: IFE-dominated quenching modulated by specific non-covalent interactions. Taken together, the data confirm that the proposed CD-based probe offers excellent anti-interference capability, enabling its reliable application in complex biological matrices and therapeutic monitoring contexts, where high selectivity is a prerequisite for accurate quantification.

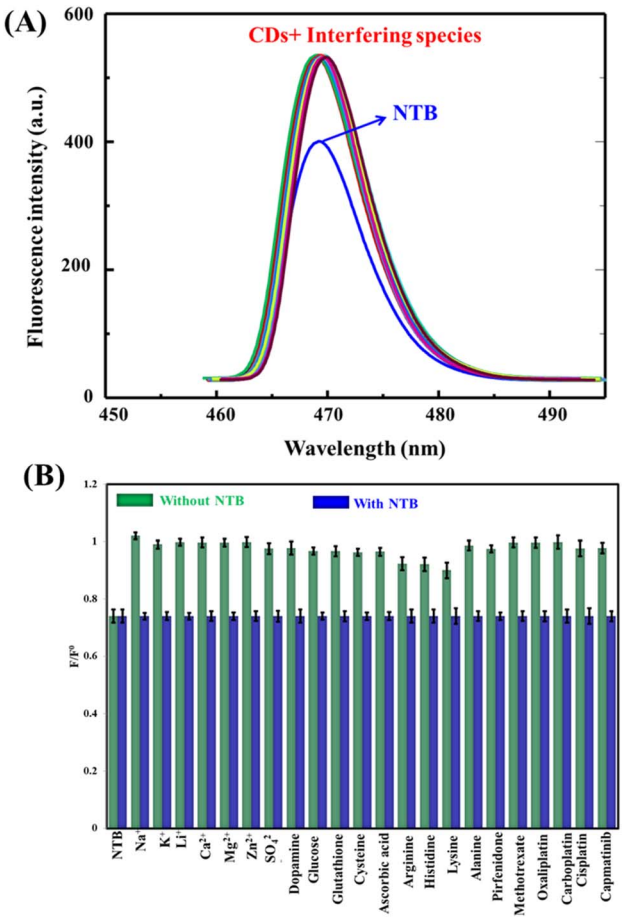

Fig. 4 Fluorescence responses (A) and corresponding bar diagram (B) of the CDs-based probe in the presence (anti-interference) and absence (selectivity) of 50 μM NTB and ten-fold of interfering species (ions, biomolecules, anti-cancer drugs). Conditions are CDs' concentration is 100 μg mL^{-1}, pH 7.4, and incubation time is 1 min.

3.7 Applications

The practical applicability of the developed CD-based probe was further validated by quantifying NTB in biological fluids. Linear calibration curves were established in serum (0.029–496.57 μM) and urine (0.014–500 μM), covering therapeutically and clinically relevant ranges. The high linearity across these matrices highlights the method's robustness in handling the complexity of biological environments. Accuracy was confirmed through recovery experiments, which yielded values between 97.6% and 103.2% (Table 3), well within the acceptance criteria for bioanalytical validation. Precision was similarly verified, with RSD values not exceeding 3.48%, demonstrating excellent reproducibility. Importantly, no statistically significant differences were observed between the proposed probe and a validated standard method,[5] underscoring the method's reliability and comparability to established analytical techniques. These findings confirm that syringe plastic-derived CDs can serve as a reliable and cost-effective platform for NTB detection in real clinical samples, supporting their potential utility in therapeutic drug monitoring, pharmacokinetic profiling, and routine clinical diagnostics. The combination of high sensitivity, accuracy, and reproducibility with operational simplicity makes the proposed method highly attractive for translation into biomedical applications.

3.8 Sustainability and energy considerations

While the upcycling of medical syringe waste into fluorescent CDs aligns with green chemistry and circular economy principles, the process involves moderate thermal inputs that warrant critical evaluation. The calcination step at 280 °C for 3 hours and the hydrothermal treatment at 200 °C for 6 hours represent energy-intensive processes. Assuming typical power consumption of 1.5 kW for muffle furnaces and 1.2 kW for hydrothermal

Table 3 Quantitative determination of NTB in spiked serum and urine samples using the CDs-based probe ($n = 3$)

		Syringe plastic-derived CDs			HPLC/UV[5]		
Matrix	Added (μM)	Found (μM)	Recovery %	RSD %	Found (μM)	Recovery %	RSD %
Human serum	0.0	—	—	—	—	—	—
	5.0	4.98	99.6	2.56	4.88	97.6	2.78
	10.0	9.78	97.8	3.19	10.47	104.7	3.43
	30.0	30.34	101.3	3.56	31.67	105.6	3.88
Human urine	0.0	—	—	—	—	—	—
	5.0	5.12	102.4	2.45	4.89	97.8	3.00
	10.0	10.32	103.2	3.08	9.67	96.7	3.56
	30.0	29.28	97.6	3.48	29.56	98.5	4.67

reactors, the combined energy usage per batch is approximately 18.6 kWh. This corresponds to a CO_2 footprint of ~14.4 kg CO_2-equivalent (assuming 0.77 kg CO_2 per kWh from grid electricity).[37–39]

However, this energy demand is partially offset by the environmental benefits of diverting single-use plastics from incineration or landfill, minimizing solvent waste, and achieving high quantum yields (46.42%) with strong batch reproducibility. Furthermore, the total synthesis is completed in less than 10 hours, and future improvements could include low-energy alternatives such as microwave or solar-assisted heating. Therefore, although not entirely energy-neutral, the method offers a realistic and scalable compromise between performance and sustainability.

3.9 "Greener" evaluation of the proposed fluorescence method

To quantitatively contextualize the 'greener' nature of the proposed method, a direct comparison with the conventional chromatographic techniques it seeks to augment is instructive. While HPLC and UPLC-MS/MS methods[5–8,31,32] offer high specificity, they are inherently resource-intensive. A typical run involves continuous pumping of organic solvents (*e.g.*, acetonitrile, methanol) through a high-pressure system for 10–20 minutes per sample, generating significant hazardous waste. Furthermore, these systems themselves are major consumers of energy, requiring constant power for pumps, ovens, and detectors (*e.g.*, MS sources), often running for hours to process a batch of samples. In contrast, the CD-based fluorometric assay presented here operates under ambient conditions without the need for high pressure or continuous solvent flow. The energy input is primarily front-loaded in the one-time synthesis of the CDs. The detection step itself is rapid (<1 min), requires only a microliter-scale aqueous buffer, and is performed on a standard fluorometer, which has a significantly lower energy footprint than an HPLC-MS/MS system. This combination of factors—minimal solvent waste, no requirement for high-purity organic solvents, lower operational energy, and a dramatically shorter analysis time—establishes a compelling case for the fluorometric method as a more sustainable and practical alternative for routine analysis, particularly in high-throughput or resource-limited settings.

4 Conclusions

In this study, we introduce a sustainable and energy-efficient strategy for synthesis of CDs derived from disposable plastic syringes. The as-prepared CDs displayed intense green fluorescence with a remarkably high quantum yield of 46.42%, reflecting their excellent optical quality. Leveraging these properties, the CDs were employed as a highly sensitive and selective fluorescent probe for the anticancer NTB, where detection was governed primarily by the IFE. The sensing platform achieved an ultralow detection limit of 2.5 nM, enabling the quantification of NTB at levels below its therapeutic plasma concentration (C_{max} ~42 nM), demonstrating suitability for trace-level detection and therapeutic monitoring. The proposed sensing platform achieved LOD of 2.5 nM, which is approximately 17 times lower than the reported therapeutic plasma concentration of NTB (C_{max} ~42 nM). While this sensitivity is sufficient for detecting sub-therapeutic levels, it does not extend several orders of magnitude below the therapeutic range. Additionally, although the method performed well in spiked biological samples, further validation using real clinical specimens and workflow simulations is necessary before routine clinical implementation. These results not only validate the analytical robustness of the system but also highlight its suitability for bioanalytical applications, therapeutic monitoring, and pharmacokinetic studies. By converting medical plastic waste into functional nanomaterials, this work proposes a pathway with a potential dual benefit: advancing nanotechnology-based sensing while offering a promising alternative for waste valorization. A full quantitative analysis of the environmental footprint, however, remains a subject for future study. The integration of high sensitivity, operational simplicity, and green synthesis renders syringe plastic-derived CDs a promising candidate for real-world biomedical analysis and clinical translation.

Ethical statement

The study received ethical approval from the Institutional Ethics Committee at the University of Assiut. Written informed consent was obtained from all participants prior to sample collection. All procedures involving human participants were conducted in accordance with the Declaration of Helsinki and applicable national regulations.

Conflicts of interest

The authors declare no competing interests.

Data availability

Data will be available upon request from the corresponding authors.

Supplementary information is available. See DOI: **https://doi.org/10.1039/d5ra07196h**.

Acknowledgements

This work was supported and funded by the Deanship of Scientific Research at Imam Mohammad Ibn Saud Islamic University (IMSIU) (grant number IMSIU-DDRSP2501).

References

1 Y. N. Lamb, *Drugs*, 2021, **81**, 575.
2 F. Amati, A. Stainer, A. Stainer, V. Polelli, M. Mantero, A. Gramegna, F. Blasi and S. Aliberti, *Int. J. Mol. Sci.*, 2023, **24**, 7849.
3 K. O. J. Kishimoto and M. Ando, *Eur. Resp. J.*, 2022, **60**, 2200380.
4 L. Wollin, E. Wex, A. Pautsch, G. Schnapp, K. E. Hostettler, S. Stowasser and M. Kolb, *Eur. Resp. J.*, 2015, **45**, 1434.
5 D. Purnachand, A. Veerareddy, B. Ramadevi, C. Kameswarrao, G. S. Reddy and B. Madhusudhanreddy, *J. Chem. Pharm. Res.*, 2015, **78**, 774.
6 S. A. Waghmare and M. Sumithra, *Anal. Chem. Lett.*, 2021, **11**, 392.
7 B. Jayagopal and S. Murugesh, *Arab. J. Chem.*, 2020, **13**, 7087.
8 B. Pasquini, S. Orlandini, S. Furlanetto, R. Gotti, M. Del Bubba, F. Boscaro, B. Bertaccini, M. Douša and G. Pieraccini, *J. Chromatogr. A.*, 2020, **1611**, 460615.
9 X. Xu, R. Ray, Y. Gu, H. J. Ploehn, L. Gearheart, K. Raker and W. A. Scrivens, *J. Am. Chem. Soc.*, 2004, **126**, 12736.
10 W. U. Khan, L. Qin, A. Alam, P. Zhou, Y. Peng and Y. Wang, *ACS Appl. Bio Mater.*, 2021, **4**, 5786.
11 H. Guo, P. Lesani, H. Zreigatac and E. J. New, *Sens. Diagn.*, 2024, **3**, 1923.
12 A. Z. Alanazi, K. Alhazzani, H. Ibrahim, A. M. Mostafa, J. Barker, A. M. Mahmoud, M. M. El-Wekil and A. B. H. Ali, *Spectrochim. Acta Part A: Mol. Biomol. Spectros.*, 2025, **325**, 125161.
13 M. H. Mahnashi, A. M. Mahmoud, M. M. El-Wekil and R. Y. Shahin, *Microchem. J.*, 2023, **193**, 109062.
14 Y. A. Bin Jardan, M. M. El-Wekil, M. R. Elmasry and A. B. H. Ali, *J. Photochem. Photobiolog. A: Chem.*, 2025, **468**, 116464.
15 J. E. Celis, W. Espejo, E. Paredes-Osses, S. A. Contreras, G. Chiang and P. Bahamonde, *Sci. Total Environ.*, 2021, **760**, 144167.
16 H. Kumar, A. Azad, A. Gupta, J. Sharma, H. Bherwani, N. K. Labhsetwar, *et al.*, *Environ. Dev. Sustain.*, 2021, **23**, 9418.
17 K. Jedruchniewicz, Y. S. Ok and P. Oleszczuk, *J. Hazard. Mater.*, 2021, **417**, 125938.
18 J. T. J. Ju, L. N. Boisvert and Y. Y. Zuo, *Adv. Colloid Interface Sci.*, 2021, **292**, 102435.
19 S. Li, J. Hu, A. A. Aryee, Y. Sun and Z. Li, *Spectrochim. Acta A Mol. Biomol. Spectrosc.*, 2023, **296**, 122659.
20 M. Kumari, G. R. Chaudhary and S. Chaudhary, *J. Mol. Liq.*, 2024, **395**, 123910.
21 A. M. Mahmoud, S. S. Abu-Alrub, A. O. Al-Qarni, B. A. Alyami, M. M. El-Wekil and M. Oraby, *Microchem. J.*, 2024, **199**, 110012.
22 Y. A. Bin Jardan, A. M. Mostafa, J. Barker, A. B. H. Ali and M. M. El-Wekil, *Anal. Methods*, 2025, **17**, 3007.
23 A. M. Mahmoud, M. H. Mahnashi, A. Al Fatease, M. A. H. Mostafa, M. M. El-Wekil and R. Ali, *J. Food Compos. Anal.*, 2022, **108**, 104428.
24 R. M. K. Mohamed, S. H. Mohamed, A. M. Asran, I. H. Alsohaimi, H. M. A. Hassan, H. Ibrahim and M. M. El-Wekil, *Spectrochim. Acta Part A: Mol. Biomol. Spectros.*, 2023, **293**, 122444.
25 S. Rajendran, D. V. Ramanaiah, S. Kundu and S. K. Bhunia, *ACS Appl. Nano Mater.*, 2021, **4**, 10931.
26 K. Kaur, S. Chaudhary, S. Singh and S. K. Mehta, *Sens. Actuators B*, 2016, **222**, 397.
27 F. P. Pandey, A. Rastogi and S. Singh, *Opt. Mater. (AMST)*, 2020, **105**, 109849.
28 M. Yang, Y. Yan, E. Liu, X. Hu, H. Hao and J. Fan, *Optical Mater*, 2021, **112**, 110743.
29 X. Wang, Y. Liu, Q. Wang, T. Bu, X. Sun, P. Jia and L. Wang, *Spectrochim. Acta Part A: Mol. Biomol. Spectros.*, 2021, **244**, 118876.
30 A. M. Mahmoud, S. S. Abu-Alrub, A. O. Alqarni, M. M. El-Wekil and A. B. H. Ali, *Microchem. J.*, 2023, **191**, 108929.
31 D. Lin, L. Qiao, Y. Zhang, Y. Liu and X. Liu, *J. Pharm. Biomed. Anal.*, 2016, **117**, 173.
32 D. Xu, Y. Zhang, J. Dai, Y. Bai, Y. Xiao and M. Zhou, *Anal. Methods*, 2015, **7**, 6561.
33 H. Subak, H. Baş and P. T. Pınar, *Diamond and Related Mater*, 2025, **153**, 112008.
34 W. Bouali, A. A. Genc, N. Erk, F. Uzcan and M. Soylak, *Electrochem. Acta*, 2025, **539**, 147097.
35 G. Magdy, A. K. El-Deen, A. S. Radwan, F. Belal and H. Elmansi, *Talanta Open*, 2025, **11**, 100423.
36 C. Dallinger, D. Trommeshauser, K. Marzin, A. Liesener, R. Kaiser and P. Stopfer, *J. Clin. Pharmacol.*, 2016, **56**, 1387.
37 U.S. Environmental Protection Agency (EPA), *Greenhouse Gas Equivalencies Calculator – Calculations and References*, Accessible date is , 2025.
38 Y. Zhou, S. Qin, S. Verma, T. Sar, S. Sarsaiya, B. Ravindran, T. Liu, R. Sindhu, A. K. Patel, P. Binod, S. Varjani, R. R. Singhnia, Z. Zhang and M. K. Awasthi, *Bioresource Techn.*, 2021, **337**, 125451.
39 M. H. Yew, A. Molla and V. Cooper, *J. Cleaner Production*, 2022, 131778.